A User's Guide to Generalized Integrate-and-Fire Models

Emerson F. Harkin, Jean-Claude Béïque, and Richard Naud

University of Ottawa Center for Neural Dynamics, Ottawa, Canada
{eharkin,jbeique,rnaud}@uottawa.ca

Computational Neuroscience Approaches to Cells and Circuits,
Michelle Giugliano, Mario Negrello, and Daniele Linaro (eds), Springer.

Contents

Abstract

The generalized integrate-and-fire (GIF) neuron model accounts for some of the most fundamental behaviours of neurons within a compact and extensible mathematical framework. Here, we introduce the main concepts behind the design of the GIF model in terms that will be familiar to electrophysiologists, and show why its simple design makes this model particularly well-suited to mimicking behaviours observed in experimental data. Along the way, we will build an intuition for how specific neuronal behaviours, such as spike-frequency adaptation, or electrical properties, such as ionic currents, can be formulated mathematically and used to extend integrate-and-fire models to overcome their limitations. This chapter will provide readers with no previous exposure to modelling a clear understanding of the strengths and limitations of GIF models, along with the mathematical intuitions required to digest more detailed and technical treatments of this topic.

Keywords: Single neuron model, Generalized integrate-and-fire model, Electrophysiology, Neuroscience, Optimization.

1 Introduction to leaky integrate-and-fire models

From an electrical perspective, a neuron is like a rubber balloon in the process of being inflated. The cell membrane of the neuron separates electrically charged ions inside and outside the cell just as the balloon separates molecules of air, and there is a difference in the distribution of charges (i.e., voltage) across the membrane of a cell just at there is a difference in pressure across the membrane of the balloon. Synaptic inputs to the neuron alter the voltage across the membrane just as adding or removing air from the balloon alters the pressure difference. The amount of air needed to appreciably change the pressure inside the balloon depends on its size, just as the number of charges needed to change the membrane voltage depends on the surface area of the membrane. If the balloon is not tied shut, the air inside will slowly leak out, just as charges leak across the cell membrane. Finally, if the difference in pressure across the rubber membrane of the balloon becomes too great, the balloon will pop, just as a neuron will fire an action potential, also called a spike, if the voltage exceeds a threshold. Once the balloon pops, the process restarts with a new, uninflated balloon, just as a neuron will reset to a lower voltage after firing an action potential.

This rubber balloon neuron model captures several of the most important electrical features of neurons, but some important details related to spiking behaviour are still missing. We will see how these can be addressed in Section 2. For now, however, we will focus on developing a mathematical description of our rubber balloon model which will serve as a foundation for the rest of the chapter.

The leaky integrate-and-fire (LIF) neuron model first introduced by Stein (1965), rooted in the work of Lapicque (1907) from over a century ago, captures the same properties of neurons as our rubber balloon analogy. The LIF models the membrane voltage $V(t)$ in terms of its rate of change dV/dt and behaviour at spike threshold V_T as follows

$$\frac{dV}{dt} = \frac{1}{C}\left(-g_l(V(t) - E_l) + I_{\text{ext}}(t)\right), \qquad V(t) < V_T \tag{1}$$

$$\begin{cases} V(t + t_{\text{ref}}) & \leftarrow V_{\text{reset}} \\ t & \leftarrow t + t_{\text{ref}} \end{cases}, \qquad V(t) \geq V_T \tag{2}$$

where g_l represents the leakiness of the membrane, which is equivalent to $1/R_m$, where R_m is the membrane resistance; E_l represents its equilibrium voltage, also called the resting membrane potential; $I_{\text{ext}}(t)$ represents external inputs to the neuron; C is the membrane capacitance, which reflects the membrane surface area; and t_{ref} is the duration of the absolute refractory period after a spike. According to Eq. 1, the membrane voltage relaxes towards its equilibrium E_l in the absence of any input $I_{\text{ext}}(t)$. This happens more quickly if the membrane is very leaky (dV/dt increases with g_l) or if the voltage is far from equilibrium (dV/dt increases with $V(t) - E_l$), and more slowly if the membrane surface area is very large (dV/dt decreases with increasing C), consistent with our balloon analogy. Whenever the voltage reaches V_T a spike occurs instantaneously, like the popping of a balloon, and the dynamics of Eq. 1 no longer apply. Instead, Eq. 2 specifies that the voltage should be reset to a lower value V_{reset} after a short refractory period t_{ref}. Unlike in many other neuron models, the membrane voltage *during* the spike is not defined—for a LIF model, a "spike" is not spike-shaped at all, it has no shape because the voltage is not defined. This simplification takes advantage of the fact that the shape of the action potential does not carry any meaningful information.

Comparison of LIF and Hodgkin-Huxley models

The decision not to model the dynamics of the membrane voltage during the action potential is one of the most important conceptual differences between LIF models, which have their roots in the early 20th-century work of Lapicque (1907), and the biophysically-realistic models first introduced by Hodgkin and Huxley (1952) half a century later.
Hodgkin and Huxley's account of the biological mechanisms of action potential generation in squid axon included a model of membrane voltage dynamics as a sum of voltage-dependent ionic currents

$$C\frac{dV}{dt} = I_{\mathrm{Na}}(t) + I_{\mathrm{K}}(t) + I_{\mathrm{ext}}(t),$$

where $I_{\mathrm{Na}}(t)$ and $I_{\mathrm{K}}(t)$ are voltage-dependent sodium and potassium currents, respectively. Unlike in Lapicque's LIF model, the membrane voltage in Hodgkin and Huxley's model is always defined, including during the action potential. This detailed and realistic approach to modelling the voltage dynamics of neurons has been enormously influential, to the point that neuron models that are based on detailed descriptions of ionic currents are commonly referred to as Hodgkin-Huxley-style models.
With the advent of more realistic and detailed Hodgkin-Huxley models, are simplified LIF models still of any use? When comparing these two types of models, it is important to keep in mind that they were created for different purposes. The original model of Hodgkin and Huxley was designed to explain how the interactions of two specific ionic currents give rise to voltage spikes with a particular shape, which we call action potentials. The original model of Lapicque, on the other hand, was created to describe how different electrical stimuli impacted the rate of action potential discharge in frog nervous tissue. For Lapicque's work, a description of the shape of the action potential (and the biophysical mechanisms responsible for it) was not necessary, and LIF models continue to be used in cases when the relationship between electrical input and the *timing* or *rate* of output spikes is of primary interest.
The negative consequences of omitting necessary biological components from a model are obvious, but there are also more subtle drawbacks of including unnecessary detail. More complicated models are usually more difficult to design and constrain to mimic specific neurons of interest, and can be liable to produce inaccurate predictions as a result (for reasons we will touch on in Section 3.1). Highly detailed models also take more time to simulate simply because more calculations are required per time step.
To summarize, LIF and Hodgkin-Huxley models each describe neurons at different levels of detail because they were created for different purposes, and each style of model comes with its own compromises.

The highly simplified LIF model provides an intuitive account of some of the most basic electrical features of neurons. In particular, the one-to-one correspondence between model parameters and fundamental properties such as resting membrane potential and spike threshold makes the LIF model straightforward to interpret. In the coming sections, we will first discuss how the LIF model can be extended to account for spike-frequency adaptation and stochastic firing in a similarly intuitive way, then show how these intuitive definitions lend themselves particularly well to being fitted to data.

2 Generalizing the leaky integrate-and-fire model

2.1 Spike-triggered adaptation

In response to a step stimulus, many neurons initially fire action potentials at a high rate which then decreases gradually to a lower rate. This phenomenon, known as spike-frequency adaptation (SFA), plays many important roles in neural systems such as enhancing the detection of weak stimuli and computing the rate of change of an input (Lundstrom et al. 2008). SFA arises from the effects of spike-triggered adaptation currents, which tend to push membrane voltage away from spike threshold, as well as the inactivation of the biophysical mechanisms that cause spiking, resulting in an effective change in the spike threshold. In this

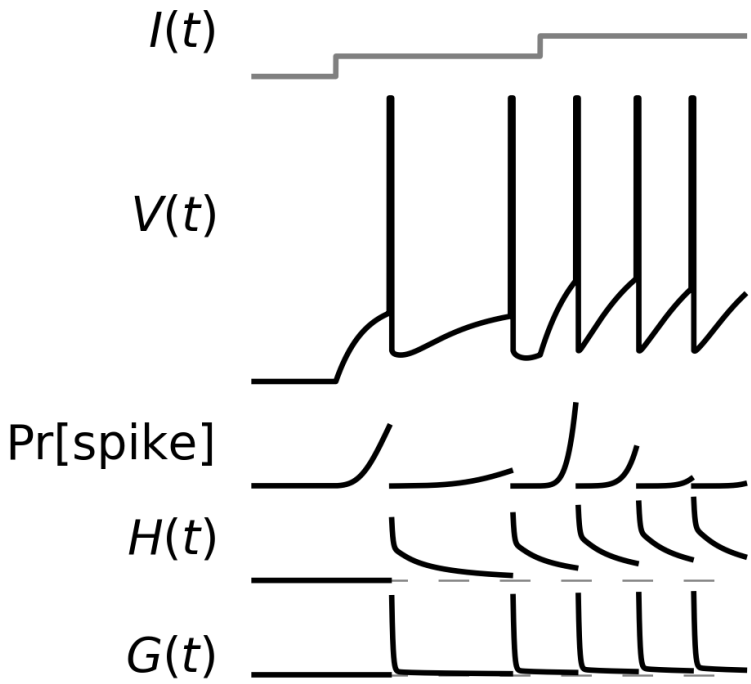

Figure 1: The generalized integrate-and-fire model. A current input $I(t)$ produces a subthreshold voltage $V(t)$ which is translated into a probability of emitting a spike Pr[spike]. Spikes are emitted stochastically and cause the voltage to reset to a lower value after a short delay, as in the leaky integrate-and-fire model. Spike frequency adaptation is caused by the spike-triggered adaptation current $H(t)$ and threshold movement $G(t)$. Notice that spikes introduce discontinuities into the spike probability and adaptation mechanisms because the dynamics of the GIF model during a spike are not defined. There are also discontinuities in the membrane voltage $V(t)$ for the same reason; however, to improve clarity, here we have set the voltage to an arbitrary high value during each spike. The dashed gray lines in $G(t)$ and $H(t)$ indicate zero.

section, we will show how to extend the LIF model to incorporate these ideas in an explicit and intuitive way.

On a conceptual level, SFA mechanisms can be divided into two categories: mechanisms which move the membrane voltage away from threshold, such as adaptation currents; and mechanisms which move the threshold away from the membrane voltage, such as inactivation of spiking mechanisms. We can capture these two categories mathematically in terms of a pair of functions $\eta(x)$ (adaptation current) and $\gamma(x)$ (threshold movement) for $x > 0$ where x is the time since a spike. In general, adaptation currents and threshold changes are large just after a spike, but fade away over time. In order to give $\eta(x)$ and $\gamma(x)$ these properties, we can define them mathematically using decaying exponentials $e^{-x/\tau}$, which fade away to zero as x increases at a rate dictated by the timescale τ. Depending on the cell type and even the individual neuron, these adaptation mechanisms may fade away quickly, slowly, or even over multiple timescales. We can accommodate this variability by implementing $\eta(x)$ and $\gamma(x)$ as *weighted sums* of exponentials with different timescales τ

$$f(x) \equiv \sum_i w_i^{(f)} e^{-x/\tau_i^{(f)}}, \qquad \tau_i^{(f)} > 0, x > 0 \tag{3}$$

where the $w_i^{(f)}$ are the weights and f corresponds to η or γ as appropriate. If a particular timescale $\tau_i^{(f)}$ is not found in a given neuron, its associated weight $w_i^{(f)}$ can simply be set to zero to remove its contribution to the overall adaptation function $f(x)$. To allow the effects of adaptation to build up over multiple spikes, we can define $H(t)$ and $G(t)$ as the sums of η and γ over the set of all past spikes $\{s \in \mathcal{S}; s < t\}$

$$H(t) \equiv \sum_{\{s \in \mathcal{S}; s < t\}} \eta\left(t - s\right) \tag{4}$$

$$G(t) \equiv \sum_{\{s \in \mathcal{S}; s < t\}} \gamma\left(t - s\right) \tag{5}$$

where $\mathcal{S}$ is the set of all spike times, s is the time of a specific spike, and t is the current time. This means that if several spikes occur in quick succession, the adaptation mechanisms $H(t)$ and $G(t)$ will be engaged more strongly than if fewer spikes had occurred. Additionally, since both η and γ go to zero as the time since a spike $t - s$ increases, past spikes contribute less and less to the adaptation functions $H(t)$ and $G(t)$ as time goes on.

The LIF neuron model presented in the previous section does not account for spike-frequency adaptation, but this is easily remedied by incorporating an adaptation current and spike-triggered threshold movement into the model via $H(t)$ and $G(t)$. In order to do that, we must first redefine the fixed spike threshold V_T to be a function $V_T(t)$ that returns the spike threshold at a specific time t, taking the effects of previous spikes into account via the threshold movement $G(t)$

$$V_T(t) \equiv V_T^* + G(t),$$

where V_T^* is the spike threshold after all adaptation has faded away. This equation shows why we call $G(t)$ the threshold movement: it gives the amount that the spike threshold has moved as a result of adaptation.

Next, we must incorporate the adaptation current $H(t)$ into the subthreshold dynamics given in Eq. 1 so that it can influence the subthreshold voltage. Simply subtracting $H(t)$ from the other currents in Eq. 1 completes the definition of our LIF model with adaptation

$$\frac{dV}{dt} = \frac{1}{C}\left(-g_l(V(t) - E_l) - H(t) + I_{\text{ext}}(t)\right), \qquad V(t) < V_T(t) \tag{6}$$

$$\begin{cases} V(t + t_{\text{ref}}) & \leftarrow V_{\text{reset}} \\ t & \leftarrow t + t_{\text{ref}}, \end{cases} \qquad V(t) \geq V_T(t). \tag{7}$$

Notice that Eq. 6 tells us that when the adaptation current $H(t)$ increases after a spike, it is subtracted away from the input current $I_{\text{ext}}(t)$. This means that the adaptation current can effectively reduce the strength of an input stimulus. Since the LIF fires less rapidly in response to weaker inputs, the adaptation current $H(t)$ causes the firing rate evoked by constant stimulus to drop off after the first few spikes, consistent with the SFA effect we seek.

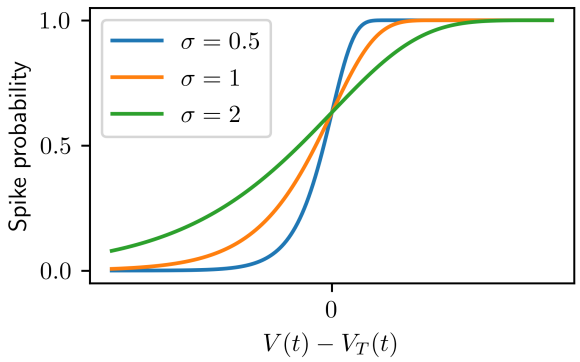

Figure 2: Typical shape of the spike probability function given in Eq. 8. The vertical axis shows the probability of spiking within a small time window $[t, t + \Delta t)$ and the horizontal axis shows the distance between the membrane voltage $V(t)$ and spike threshold $V_T(t)$. Notice that increasing the stochasticity scaling factor σ increases the probability of spiking below threshold. The spike probability function shown here is $\rho\left(\frac{V(t)-V_T(t)}{\sigma}\right) = \exp\left[-e^{\frac{V(t)-V_T(t)}{\sigma}}\Delta t\right]$, which is used by the GIF model as previously described (Mensi, Naud, et al. 2012; Gerstner et al. 2014; Pozzorini et al. 2015; Mensi, Hagens, et al. 2016; Harkin et al. 2020).

2.2 Stochasticity

The LIF model presented here fires a spike instantaneously when the voltage exceeds a threshold $V_T(t)$, but in real neurons this process is less precise (Mainen and Sejnowski 1995). In general, neurons are more *likely* to spike when their membrane voltage exceeds a threshold, but it is also possible for spikes to occur when the voltage is below threshold or vice-versa. It can therefore be helpful to think of the relationship between voltage and spiking in terms of a *probability* that depends on the current voltage and threshold, rather than as a hard cutoff. We can express this idea mathematically in terms of a spike probability function

$$\rho\left(\frac{V(t) - V_T(t)}{\sigma}\right) = \Pr[\text{spike between time } t \text{ and } t + \Delta t \mid V(t) - V_T(t)], \tag{8}$$

where $\Pr[x \mid y]$ denotes the probability of x given y, σ is a scaling factor that sets the degree of stochasticity, and Δt is a small time interval. To capture our intuition that spikes are more likely when $V(t)$ is above $V_T(t)$, $\rho\left(\frac{V(t)-V_T(t)}{\sigma}\right)$ is usually a sigmoidal function that is close to 1 when $V(t) - V_T(t) > 0$ and close to 0 when $V(t) - V_T(t) < 0$, such as the one shown in Fig. 2. The scaling factor σ allows us to control how quickly the probability of spiking increases when the voltage is above threshold. In more intuitive terms, σ sets the threshold *sharpness*.

Incorporating this stochastic spiking behaviour into the LIF model with adaptation will complete our definition of the generalized integrate-and-fire model (GIF). To accomplish this, we simply need to invoke the spiking rule given in Eq. 7 *probabilistically* according to the spike probability function given in Eq. 8 rather than deterministically whenever the voltage exceeds a given threshold. The pseudocode in Algorithm 1 sketches how this can be done, and an example of a model simulated this way is shown in Fig. 1.

2.3 Simplifications, generalizations, and limitations

The generalized integrate-and-fire model we have presented here accounts for more features of neuronal excitability than the leaky integrate-and-fire model from Section 1, but it is still a highly simplified model. Compared with the LIF model, the GIF model accounts for two important phenomena related to spiking: spike-triggered adaptation and a stochastic threshold. However, the GIF model does not account for subthreshold adaptation that is not related to spiking, nor does it account for the effects of the mechanisms that give rise to stochastic spiking on the subthreshold voltage.

Algorithm 1 Simulation procedure for the GIF model.

Require: $I_{\text{ext}}(t)$ ▷ Input current.
Require: $C, g_l, E_l, \eta, \gamma, V_T^*, \sigma, \rho$ ▷ Model components.
Require: $V_0, \Delta t, T$ ▷ Initial voltage, simulation timestep, and duration of simulation.
Require: $\xi(t)$ ▷ Random number between 0 and 1 sampled at time t.

▷ Set initial condition.
$t \leftarrow 0$
$V(t) \leftarrow V_0$
$\mathcal{S} \leftarrow \{\emptyset\}$
while $t < T$ **do**
  $G(t) \leftarrow \sum_{\{s \in \mathcal{S}; s<t\}} \gamma(t-s)$ ▷ Compute threshold movement from Eq. 5.
  $V_T(t) \leftarrow V_T^* + G(t)$ ▷ Compute spike threshold with adaptation.
  if $\xi(t) \leq \rho\left(\frac{V(t)-V_T(t)}{\sigma}\right)$ **then**
    $\mathcal{S} \leftarrow \mathcal{S} \cup t$ ▷ Add t to the set of spike times.
    ▷ Emit a spike according to Eq. 7.
    $V(t+t_{\text{ref}}) \leftarrow V_{\text{reset}}$
    $t \leftarrow t + t_{\text{ref}}$
  else
    $H(t) \leftarrow \sum_{\{s \in \mathcal{S}; s<t\}} \eta(t-s)$ ▷ Compute adaptation current from Eq. 4.
    ▷ Integrate membrane dynamics from Eq. 6
    $\Delta V \leftarrow \frac{\Delta t}{C}\left(-g_l(V(t)-E_l) - H(t) + I_{\text{ext}}(t)\right)$
    $V(t+\Delta t) \leftarrow V(t) + \Delta V$
    $t \leftarrow t + \Delta t$ ▷ Increment time.
  end if
end while
return $V(t), \mathcal{S}$ for $0 \leq t < T$

Subthreshold adaptation can be produced by voltage-activated currents that oppose the very changes in voltage that cause them to activate, creating the appearance of a sag in the voltage response to step inputs. Prominent examples include the hyperpolarization-activated current I_h and subthreshold voltage-activated potassium currents. From a functional perspective, the main effect of these currents is to filter out inputs that produce slow changes in voltage, while letting through inputs that cause the voltage to change quickly. In real neurons, this frequency filtering effect is specific to the range of subthreshold voltages in which the current activates — if an input current produces a change in voltage that does not activate the current causing subthreshold adaptation, no adaptation is produced. In GIF models, subthreshold adaptation is most easily accounted for by adding a slowly activating leak current. This approach is mathematically simple to implement but disregards potential voltage-specificity of subthreshold adaptation. An alternative approach is to augment the GIF model with explicit Hodgkin-Huxley models of the currents that give rise to adaptation. We will discuss how to augment GIF models with Hodgkin-Huxley components in Section 3.4.

Stochastic firing in real neurons arises partly from the fast but not instantaneous dynamics of the sodium channels that mediate spiking. In real neurons, sodium channels begin to open when the membrane potential approaches threshold. This pushes the membrane potential even closer to threshold, creating a positive feedback loop between membrane potential and sodium channel activation. Eventually, this process passes a threshold or point of no return and a spike is produced. In the GIF model, this soft positive feedback process is replaced by a probability of spiking. When the positive feedback process is strong enough to very rapidly pass the point of no return (i.e., when the threshold is very sharp), the probabilistic threshold of the GIF model can be a good approximation. However, if this positive feedback process is initially very weak, the activity of sodium channels can impact the subthreshold voltage dynamics without leading to spiking. In this case, the probabilistic threshold of the GIF model is a worse approximation because it does not capture the effects of spiking mechanisms on the subthreshold dynamics.

The GIF model differs from real neurons in one additional important respect: real neurons exhibit a complex morphological structure, but the GIF model represents a voltage at a single point. The GIF model is most accurate when only inputs and outputs at the level of the cell body are considered. Fortunately, an electrode located at the cell body is often both the main source of input and instrument for measuring output during *in vitro* electrophysiological experiments. Unfortunately, under physiological conditions, most of the input to a neuron arrives via synapses located on potentially electrically-distant dendrites, and the point-neuron simplification of the GIF model may be less appropriate.

In sum, while the GIF model offers a simple and intuitive description of many of the electrical properties of neurons, it does not capture *all* of the properties of neurons equally well. When the subthreshold effects of ionic currents, spiking mechanisms, or neuronal morphology are of primary interest, it is important to consider whether the GIF model can be adapted to account for these mechanisms to a satisfactory extent, or whether an entirely different modelling framework should be chosen.

3 Fitting the generalized integrate-and-fire model

3.1 Finding parameter values: experiments vs. optimization

So far we have presented the GIF model as an intuitive single neuron model formulated in terms of interpretable input and output *variables*, which include input current, voltage, and spike times, and *parameters*, such as membrane leakiness and spike threshold. Next, we turn to the question of how to choose appropriate values for the parameters. In practice, there are two main approaches: carry out a series of detailed electrophysiological experiments to measure each parameter in the model, for example, by applying current steps of various amplitudes to measure the action potential threshold, or use mathematical optimization techniques to find the parameter values that cause the output of the model to mimic that of a real neuron. Choosing between these two approaches involves a trade-off between the interpretation of model parameters and the accuracy of model predictions. Following the experimental approach, parameter values will have a precise and familiar physiological interpretation, but the output of the model might not mimic that of any particular neuron or cell type very closely. Following the optimization-based approach, the parameter values will represent effective quantities with a potentially less precise physiological interpretation, but the output predicted by the model will match that of a particular neuron as closely as possible. For readers with a strong background in experimental neuroscience, it may come as a surprise that models constructed using

experimentally-measured parameter values can produce poor predictions in common cases. In this section, we discuss why this happens and present an alternative optimization-based approach.

One situation in which models constructed using experimentally-measured parameter values produce poor predictions arises when both of the following conditions are met:

1. the true values of the parameters in the neuron population of interest are correlated or are otherwise not statistically independent, and

2. it is not possible to experimentally determine the values of all of the parameters in a single neuron, or this data is not available even if it is possible to collect.

This situation arises very often in practice. This is partly because the first condition is surprisingly easy to meet since it is sufficient for only two of the model parameters to be related (resting membrane potential and action potential threshold, for instance). The second condition is also usually met because it is often impractical to measure each of the model parameters in every neuron, even if it is technically possible. If both conditions are met, the distribution of the experimentally-determined model parameters will not match the true distribution in the population. Since the behaviour of the GIF model is controlled by its parameters, this can easily lead to models that exhibit unexpected behaviours that are not found in the population of neurons they are intended to mimic.

To see why, consider a hypothetical population of neurons with a similar degree of spike frequency adaptation. Suppose that this adaptation is caused by a variable mixture of an adaptation current and moving threshold, but that the sizes of the adaptation current and moving threshold are anticorrelated such that the overall degree of spike frequency adaptation is roughly constant. If it is not possible to measure both the adaptation current and moving threshold in the same neurons, a researcher might observe that both the adaptation and moving threshold range from small to large, but not realize that they are anticorrelated. This might lead them to create a set of models that includes neurons with both a large moving threshold and adaptation current, even though no such neurons exist in the population. As a result, the models might exhibit more variable spike frequency adaptation than the neuron population (Balachandar and Prescott 2018). Even if the researcher decides to create a single model of an "average" neuron by setting both the adaptation current and moving threshold to a moderate amplitude, the degree of spike frequency adaptation in the model might be very different from any of the neurons in the population. This is because the non-linear interactions between the adaptation current and moving threshold cause the total amount of spike frequency adaptation to be different from the sum of its parts. Similarly, the average spike frequency adaptation in a population can be different from the averages of its parts. This phenomenon is sometimes called the failure of averaging (Golowasch et al. 2002).

In an alternative approach to parameter estimation, an experimenter records the voltage response of a neuron to an input current delivered via an intracellular electrode and the output of the model in response to the same input is forced to match that of the neuron as closely as possible (Pozzorini et al. 2015). This approach involves defining a mathematical measure of similarity between the output of the model and the observed behaviour of a neuron and finding a set of parameter values that maximize this measure. In some cases, it is possible to find the similarity-maximizing parameter values directly by taking advantage of mathematical properties of the similarity measure. However, it is often necessary to simply take an initial guess at the values of the model parameters and then adjust them repeatedly in the direction of increasing similarity until a maximum level of similarity is reached, a process known as gradient ascent. Whether they are obtained via gradient ascent or found directly, the similarity-maximizing values are referred to as the *optimal* values for the corresponding parameters, and the process of finding them is called *optimization* or fitting.

The optimization process can be understood more intuitively by visualizing it in terms of a similarity landscape. If we focus on only two of the model parameters at a time, we can imagine that the two parameters give the latitude and longitude of a point on this landscape and that the similarity defines the altitude of that point. Following this analogy, points of maximal similarity correspond to the tops of hills in this landscape. We can imagine gradient ascent as the process of starting somewhere on the landscape and proceeding uphill. In the machine-learning literature, it is more common to define a mathematical measure of dissimilarity and use gradient descent to find optimal points lying at the bottoms of valleys; for the sake of simplicity, we will focus on similarity/gradient ascent for now. Depending on the model and similarity measure, there can be

more than one hill in the similarity landscape[1]. When this is the case, finding the point at the top of the tallest hill becomes quite difficult because we cannot reach it by proceeding uphill from any starting point. (Fortunately, in the case of the GIF model, there is only one hill and finding the parameter values that produce the highest possible similarity is not difficult[2].) This process works the same way when there are more than two parameters, but visualizing a landscape with additional dimensions stretches the imagination.

The main advantages of this optimization-based approach over experimentally determining parameter values are that optimization is less labour intensive and yields models that produce more accurate predictions. On the other hand, a potential drawback of this approach is that the parameter values obtained via optimization do not necessarily correspond exactly to experimental measurements. To see why, consider a neuron that is exactly like the GIF model except that it has an additional voltage-dependent conductance

$$\frac{dV}{dt} = \frac{1}{C}\left(-g_l(V(t) - E_l) - g_v(V)(V(t) - E_l) - H(t) + I(t)\right),$$

where $g_v(V)$ is the voltage-dependent conductance. If a researcher were to fit the GIF model to this neuron, the effect of the voltage-dependent conductance would be mixed into the leak conductance of the GIF model

$$-g_l(V(t) - E_l) - g_v(V)(V(t) - E_l) = -(g_l + g_v(V))(V(t) - E_l) \implies \hat{g}_l = g_l + g_v(V),$$

where $\hat{g}_l$ is the value obtained by fitting the GIF model. Notice that not only is there a mismatch between the fitted leak conductance and the true leak conductance of the neuron, $\hat{g}_l \neq g_l$, but, since $g_v(V)$ depends on voltage and $\hat{g}_l = g_l + g_v(V)$, the value obtained for $\hat{g}_l$ depends on the voltage of the neuron! This illustrates that unless the neuron to which the GIF model is fitted *is* a GIF model, the optimal parameter values should not be interpreted as exact substitutes for experimentally-determined values. Instead, they should be interpreted as *effective* values, in the sense that they specify how much a particular variable affects the output of the GIF model within the context of a specific input and set of model components.

The mismatch between optimal model parameter values and experimental measurements is hardly unique to the GIF model. In fact, it arises to some extent in all models that are not exact copies of the systems they are intended to mimic. (Such a model would, of course, be of very little use!) Model simplification involves combining multiple components of a more complex model into a smaller number of components in a simpler model, often introducing approximations in the process. This might seem to suggest that more accurate parameter values could be obtained by fitting models with fewer simplifications, but in practice this is not often the case. Complex neuron models with detailed representations of the elaborate morphology or diverse ionic composition of real neurons are very difficult to fit to data because these complexities introduce many hills and valleys into the similarity landscape, making the best parameter values hard to find.

In this chapter, we will focus on an optimization-based approach for determining parameter values mainly because GIF models constructed in this way yield more accurate predictions of neural output. In addition, the fact that all of the parameters in the GIF model can be fitted simultaneously to small amounts of data means that the optimized values of those parameters provide a detailed window into the effective properties of *individual cells*. However, the reader should be aware that GIF model parameter estimates obtained via optimization come with important caveats: value estimates may depend on the conditions under which they were obtained (for example, the voltage range, as discussed above) and the extent to which the GIF model resembles the neuron being fitted. In the coming sections, we will show how each of these caveats can be addressed.

3.2 Choosing an input

Optimization-based methods for choosing GIF model parameter values involve matching the output of the GIF model to that of a real neuron for a given input. How, then, to choose the input? More importantly, why does the choice of input matter? In Section 3.1, we saw that the parameter values found via optimization

[1] In this case, the points at the tops of hills are higher than all points within a small neighbourhood, but not necessarily all points in the landscape. After all, there might be taller hills elsewhere. Points that are only optimal within a small neighbourhood are called locally optimal and the point at the top of the tallest hill is called *globally* optimal.

[2] Although the measures of similarity and dissimilarity used by the GIF model will be presented briefly in Section 3.3, the reasons that these measures are associated with landscapes that have a particular structure are beyond the scope of this chapter. For a thorough introduction, see (Paninski, Simoncelli, and Jonathan W Pillow 2004; Gerstner et al. 2014).

can depend on the range of voltages experienced by the neuron to which the GIF model is fitted. Since the voltage of a neuron depends on its input, the parameter values found via optimization depend on the input as well. This implies that the choice of input is important for two reasons: first, the effective parameter values found by fitting the GIF model are specific to the input used during fitting; second, since the predictions made by the GIF model depend on the values of its parameters, the neuronal outputs (i.e., voltage, spike times) predicted by the GIF model are most accurate for the input used during fitting.

Whether the GIF model is to be used to predict neuronal outputs or gain insight into the effective properties of individual cells, both goals are more easily accomplished when the input used for fitting the GIF model is chosen appropriately. Which input is most appropriate depends on the research question at hand; each researcher must ask themselves whether specific types of input (e.g., synaptic vs. artificial), frequency bands (e.g., θ oscillations), or voltage ranges (e.g., close to action potential threshold) are most relevant to their question. In practice, however, noise is often used as input because the fluctuations present in noise cover a wide range of simpler inputs (slow rise, fast rise, rise-then-fall, etc.). Ornstein-Uhlenbeck noise is a particularly popular choice because it approximates the random fluctuations produced by the synaptic bombardment neurons receive *in vivo* (Pozzorini et al. 2015).

Carefully selecting the input used to fit the GIF model, or simply using noise, mitigates one of the important caveats associated with GIF models; namely, that parameter estimates — and, by association, model predictions — are somewhat specific to a given input. The degree of specificity can be quantified by simply comparing the parameter estimates or predictions on different subsets of data collected from a given neuron (Pozzorini et al. 2015). In the machine learning literature, it is common to divide a dataset of independent samples into a portion used for fitting a model and a separate portion for testing the accuracy of model predictions using new inputs, referred to as the training and test datasets, respectively. In the case of data used to fit the GIF model, completely independent samples are difficult to obtain due to the long-lasting effects of adaptation mechanisms. In practice, nearly independent samples of neuronal output are obtained by applying at least two distinct inputs to each neuron to be fitted, each separated by an equilibration period of several seconds. The data associated with some of the inputs will be used for fitting while the rest is reserved for testing, effectively dividing the experiment into separate training and test phases. Since our goal is to evaluate the accuracy of GIF model predictions on the test input, the experimenter should attempt to ensure that the training and test phases of the experiment are as similar as possible apart from the choice of input. For a detailed discussion of the best practices for evaluating the accuracy of GIF models, see Pozzorini et al. (2015). For a more general treatment of model selection and accuracy estimation, see Hastie, Tibshirani, and Friedman (2009) and Kohavi (1995).

3.3 Optimization

3.3.1 Quantifying model accuracy

All optimization techniques rely on a precise definition of the similarity or dissimilarity between the actual and desired outputs of a function. In the case of the GIF model, this means we must define how we will measure the similarity between the output of the GIF model and that of a real neuron. Because the GIF model is divided into two parts, each with their own outputs and parameters, we will in fact need to define two separate measures: one for the subthreshold component of the model, and one for the stochastic spiking rule.

The subthreshold component of the GIF model given in Eq. 6 defines the relationship between an external input $I_{\text{ext}}(t)$ and the derivative of the membrane voltage $\widehat{\frac{dV}{dt}}$ given the current voltage of the neuron $V(t)$ and the timing of spikes $\mathcal{S}$. Notice that we have added a hat $\widehat{\ }$ to the voltage derivative to indicate that this quantity is predicted by the model rather than measured experimentally. We take the subthreshold voltage $V(t)$ and the set of spike times $\mathcal{S}$ to be given because they are easily measured experimentally, and because doing so allows us to isolate the effect of the *parameters* of the subthreshold model $\hat{g}_l$, $\widehat{E}_l$, $\widehat{C}$, $\widehat{w}_i^{(\eta)}$, and $\widehat{\tau}_i^{(\eta)}$ on its output $\widehat{\frac{dV}{dt}}$. Because the voltage derivative is a continuous signal, we can quantify the level of dissimilarity between the predicted derivative $\widehat{\frac{dV}{dt}}$ and the experimentally measured derivative $\frac{dV}{dt}$ using the

sum of squared errors

$$J(\hat{g}_l, \widehat{E}_l, \widehat{C}, \widehat{w}_1^{(\eta)}, \ldots, \widehat{w}_k^{(\eta)}, \widehat{\tau}_1^{(\eta)}, \ldots, \widehat{\tau}_k^{(\eta)}; I(t), \mathcal{S}, V(t)) = \sum_{t \notin \mathcal{S}'} \left(\frac{dV}{dt} - \widehat{\frac{dV}{dt}} \right)^2, \tag{9}$$

where $t \notin \mathcal{S}'$ is time excluding a small window around each spike. Notice that if we choose values of the parameters $\hat{g}_l$, $\widehat{E}_l$, etc. that cause the predicted voltage derivative $\widehat{\frac{dV}{dt}}$ to be far above or below the measured derivative $\frac{dV}{dt}$, this dissimilarity function will have a large value. On the other hand, if we choose parameter values that cause the output of the model to match the measured derivative exactly, the dissimilarity will be zero. Our objective is therefore to find the parameter values that minimize $J(\hat{g}_l, \ldots; I(t), \mathcal{S}, V(t))$, which can be expressed mathematically as

$$\underset{\hat{g}_l, \widehat{E}_l, \widehat{C}, \widehat{w}_1^{(\eta)}, \ldots, \widehat{w}_k^{(\eta)}, \widehat{\tau}_1^{(\eta)}, \ldots, \widehat{\tau}_k^{(\eta)}}{\arg\min} J\left(\hat{g}_l, \widehat{E}_l, \widehat{C}, \widehat{w}_1^{(\eta)}, \ldots, \widehat{w}_k^{(\eta)}, \widehat{\tau}_1^{(\eta)}, \ldots, \widehat{\tau}_k^{(\eta)}; I(t), \mathcal{S}, V(t)\right)$$

where $\arg\min_x f(x)$ finds the value of x that minimizes $f(x)$. This notation is common in the machine learning literature, in which $J(x)$ is referred to as an objective function or loss function.

The stochastic spiking rule given in Eq. 8 defines the probability of emitting a spike at a particular time t given the subthreshold voltage predicted by the model $\widehat{V}(t)$ and the timing of previous spikes $\{s \in \mathcal{S}; s < t\}$ (indirectly through Eq. 5). Our goal is therefore to find values for the parameters in the spiking rule $\widehat{V}_T^*$, $\widehat{\sigma}$, $\widehat{w}_i^{(\gamma)}$, and $\widehat{\tau}_i^{(\gamma)}$ that maximize the probability that the spikes emitted by the model occur at the same time as spikes are observed experimentally

$$\underset{\widehat{V}_T^*, \widehat{\sigma}, \widehat{w}_1^{(\gamma)}, \ldots, \widehat{w}_k^{(\gamma)}, \widehat{\tau}_1^{(\gamma)}, \ldots, \widehat{\tau}_k^{(\gamma)}}{\arg\max} \Pr\left[\widehat{\mathcal{S}} = \mathcal{S} \mid \widehat{V}(t)\right]$$

where $\widehat{\mathcal{S}}$ and $\mathcal{S}$ are the model predicted and experimentally observed sets of spike times, respectively. More precisely, we would like to maximize the joint probability that the model emits a spike when a spike is observed experimentally and that the model does not emit a spike when a spike is not observed experimentally

$$\Pr\left[\widehat{\mathcal{S}} = \mathcal{S} \mid \widehat{V}(t)\right] = \Pr\left[\bigcap_t \begin{cases} t \in \widehat{\mathcal{S}} \text{ if } t \in \mathcal{S} \\ t \notin \widehat{\mathcal{S}} \text{ if } t \notin \mathcal{S} \end{cases} \middle| \widehat{V}(t) \right].$$

Unfortunately, the probability that the model emits a spike at a particular time t depends on the timing of previous spikes $\{\hat{s} \in \widehat{\mathcal{S}}; \hat{s} < t\}$ due to spike frequency adaptation induced by the moving threshold $G(t)$ from Eq. 5. This means that the probabilities that the model does or does not emit a spike at any particular set of times $t_i, t_j, t_k, \ldots$ are not independent, and consequently we cannot write the previous equation as a product of probabilities. However, if we assume that all of the spikes up to a given time t were emitted at the correct times $\{\hat{s} \in \widehat{\mathcal{S}}; \hat{s} < t\} \leftarrow \{s \in \mathcal{S}; s < t\}$, then we can take advantage of the fact that the spiking probabilities under this assumption are independent to rewrite the previous equation using the product rule

$$\Pr\left[\widehat{\mathcal{S}} = \mathcal{S} \mid \widehat{V}(t)\right] = \prod_t \begin{cases} \rho\left(\frac{\widehat{V}(t) - \widehat{V}_T(t)}{\widehat{\sigma}}\right) & \text{if } t \in \mathcal{S} \\ 1 - \rho\left(\frac{\widehat{V}(t) - \widehat{V}_T(t)}{\widehat{\sigma}}\right) & \text{if } t \notin \mathcal{S} \end{cases} \tag{10}$$

where $\rho\left(\frac{\widehat{V}(t) - \widehat{V}_T(t)}{\widehat{\sigma}}\right)$ gives the probability of spiking at time t (see Eq. 8). This gives us a concrete expression for the similarity between the output of the spiking rule of the GIF model and the experimentally observed spike times which we can maximize.

3.3.2 Solving for parameter values

Now that we have expressed the degree of agreement between the outputs of the GIF model and of a real neuron, we can turn to the question of how to adjust the model parameters to minimize the dissimilarity in Eq. 9 and maximize the similarity in Eq. 10. If we fix the timescales $\tau_1^{(\eta)}, \ldots, \tau_k^{(\eta)}, \tau_1^{(\gamma)}, \ldots, \tau_k^{(\gamma)}$, we can solve

for the remaining parameters to minimize this restricted form of Eq. 9 directly, and maximize the restricted form of Eq. 10 by gradient ascent.

It is possible to solve for the optimal values of the unknown parameters in Eq. 9 because the term representing the subthreshold dynamics of the GIF model $\widehat{\frac{dV}{dt}}$ can be rewritten as a linear equation. The parameter values that minimize the sum of squared errors of any linear model can be found using ordinary least-squares regression. Simple linear models include $\hat{y} = \hat{m}x + \hat{b}$ for a single input variable x, or

$$\hat{y} = \widehat{\beta}_0 + \widehat{\beta}_1 x_1 + \widehat{\beta}_2 x_2 + \ldots + \widehat{\beta}_n x_n$$

for n input variables. The $\widehat{\beta}_i$ are called regression coefficients or model parameters. In a geometric interpretation of this equation, $\widehat{\beta}_0$ is called an intercept and $\widehat{\beta}_1, \ldots, \widehat{\beta}_n$ are called slopes. It might not be immediately obvious that the GIF model is such a linear model, but if the subthreshold dynamics from Eq. 6 are expanded and rearranged, we obtain the following

$$\widehat{\frac{dV}{dt}} = \frac{\widehat{g}_l \widehat{E}_l}{\widehat{C}} + \frac{-\widehat{g}_l}{\widehat{C}} V(t) + \frac{1}{\widehat{C}} I_{\text{ext}}(t) + \frac{-\widehat{w}_1^{(\eta)}}{\widehat{C}} \sum_{\{s \in \mathcal{S}; s<t\}} e^{\frac{s-t}{\tau_1^{(\eta)}}} + \cdots + \frac{-\widehat{w}_k^{(\eta)}}{\widehat{C}} \sum_{\{s \in \mathcal{S}; s<t\}} e^{\frac{s-t}{\tau_k^{(\eta)}}}$$

which can be rewritten as

$$\hat{y} = \widehat{\beta}_0 + \widehat{\beta}_1 V(t) + \widehat{\beta}_2 I_{\text{ext}}(t) + \widehat{\beta}_3 \sum_{\{s \in \mathcal{S}; s<t\}} e^{\frac{s-t}{\tau_1^{(\eta)}}} + \cdots + \widehat{\beta}_{k+2} \sum_{\{s \in \mathcal{S}; s<t\}} e^{\frac{s-t}{\tau_k^{(\eta)}}}, \tag{11}$$

where $\widehat{C} = 1/\widehat{\beta}_2$, $\widehat{g}_l = -\widehat{\beta}_1/\widehat{\beta}_2$, and so on. This is a linear model where the output $\hat{y} = \widehat{\frac{dV}{dt}}$ is the voltage derivative; the inputs x_i are the injected current $I_{\text{ext}}(t)$, the subthreshold voltage $V(t)$, and the exponential basis functions of the adaptation current $\eta(t-s)$ from Eq. 3 summated over past spikes $\{s \in \mathcal{S}; s < t\}$ (obtained by decomposing $H(t)$ from Eq. 4); and the regression coefficients $\widehat{\beta}_i$ are the unknown parameters. This linear form of the subthreshold dynamics shows why it is necessary to fix the values of $\tau_i^{(\eta)}$: if these values were not fixed, the dynamics could not be written in terms of known input variables multiplied by unknown regression coefficients, and it would not be possible to use ordinary least squares regression to estimate all of the unknown parameters. Importantly, this form also shows that more components can be added to the subthreshold part of the GIF model as long as they can be written in terms of a known variable scaled by an unknown amount (this will be discussed in detail in Section 3.4).

Unfortunately, there are no similar techniques to find the values of the threshold parameters that maximize Eq. 10 directly. Instead, we must begin with a set of initial guesses for the values of these parameters and incrementally improve them using gradient ascent. In practice, the spike probability function used in the GIF model, $\rho(\frac{\widehat{V}(t) - \widehat{V}_T(t)}{\widehat{\sigma}})$ (see Eq. 8), guarantees that gradient ascent will eventually lead us to the best possible values for these parameters (Paninski, Simoncelli, and Jonathan W Pillow 2004; "Estimating parameters of probabilistic neuron models" 2014). Similarly to the subthreshold optimization process discussed above, this guarantee is subject to certain constraints, and the simplest way to satisfy these constraints is to require that the term inside the spike probability function, $\frac{\widehat{V}(t) - \widehat{V}_T(t)}{\widehat{\sigma}}$ in this case, can be written as a linear function of its parameters. By expanding $\widehat{V}_T(t)$ and rearranging, we can rewrite the term inside the spike probability function as

$$\begin{aligned}
\frac{\widehat{V}(t) - \widehat{V}_T(t)}{\widehat{\sigma}} &= \frac{-\widehat{V}_T^*}{\widehat{\sigma}} + \frac{1}{\widehat{\sigma}} \widehat{V}(t) + \frac{-\widehat{w}_1^{(\gamma)}}{\widehat{\sigma}} \sum_{\{s \in \mathcal{S}; s<t\}} e^{\frac{s-t}{\tau_1^{(\gamma)}}} + \cdots + \frac{-\widehat{w}_k^{(\gamma)}}{\widehat{\sigma}} \sum_{\{s \in \mathcal{S}; s<t\}} e^{\frac{s-t}{\tau_k^{(\gamma)}}} \\
&= \widehat{\beta}_0 + \widehat{\beta}_1 \widehat{V}(t) + \widehat{\beta}_2 \sum_{\{s \in \mathcal{S}; s<t\}} e^{\frac{s-t}{\tau_1^{(\gamma)}}} + \cdots + \widehat{\beta}_{k+2} \sum_{\{s \in \mathcal{S}; s<t\}} e^{\frac{s-t}{\tau_k^{(\gamma)}}},
\end{aligned}$$

where $\widehat{V}(t)$ is the voltage predicted by the subthreshold component of the model. This expression for $\frac{\widehat{V}(t) - \widehat{V}_T(t)}{\widehat{\sigma}}$ is of course linear with respect to the unknown parameters. Just as with the subthreshold component of the model, this linear form illustrates that additional components can be added to the spiking rule of the GIF model as long as they can be written as a known variable scaled by an unknown amount.

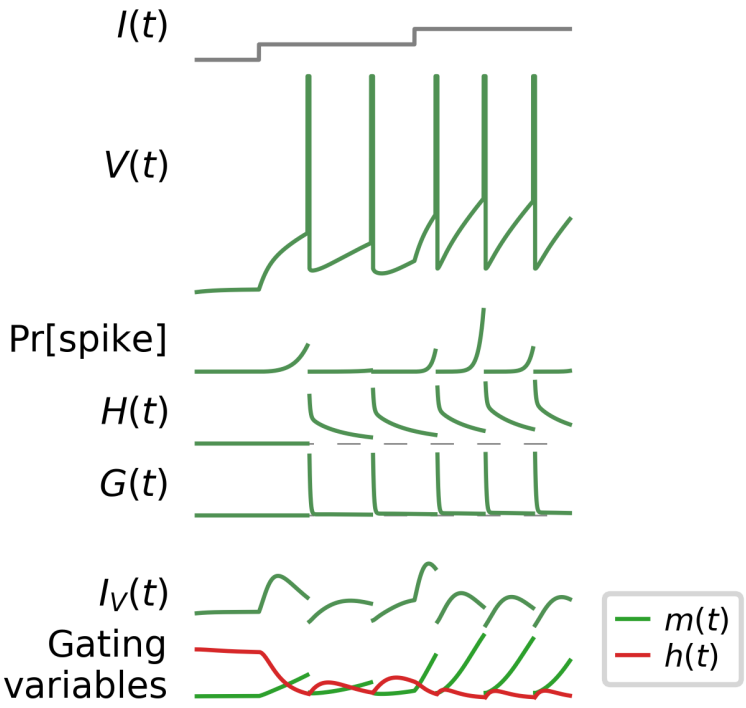

Figure 3: A GIF model augmented with a voltage-dependent current.

3.4 Extending the subthreshold model

The GIF model, like all other neuron models, is subject to the No Free Lunch theorem: no single model is best for all cases (Wolpert and Macready 1997). The simplifications used to construct the GIF model — for example, that the subthreshold dynamics of neurons are not voltage-dependent — might present problems for particular cell types or research questions. In this section, we will use the serotonin neurons of the dorsal raphe nucleus as a case study to illustrate how the GIF model can be extended to address limitations of the subthreshold model.

The subthreshold electrical properties of serotonin neurons are characterized by an unusually large membrane resistance (equivalent to a very small leak conductance) and a potent voltage-dependent ionic current (Harkin et al. 2020). These characteristics violate one of the core assumptions of the GIF modelling framework, namely, that the subthreshold electrical properties of neurons are dominated by a voltage-independent leak conductance. Fortunately, it is possible to augment the subthreshold dynamics of the GIF model with a voltage-dependent component to account for the specific characteristics of serotonin neurons. To see how, we will start by adding a voltage-dependent current $I_V(t)$ to the subthreshold dynamics of the GIF model defined in Eq. 6

$$\frac{dV}{dt} = \frac{1}{C}\left(-g_l(V(t) - E_l) + I_V(t) - H(t) + I_{\text{ext}}(t)\right). \tag{12}$$

We can model $I_V(t)$ following the usual Hodgkin-Huxley approach

$$I_V(t) = g_V m(t) h(t)(V(t) - E_V) \tag{13}$$

where g_V is the maximum conductance; $m(t)$ and $h(t)$ are activation and inactivation gating functions, respectively; and E_V is the reversal potential of the current. The details of the gating functions and reversal potential are not important; suffice it to say that these can usually be determined experimentally[3] or controlled. With this in mind, we can group together the known terms from Eq. 13 into a new variable

[3]The gating functions in Hodgkin-Huxley current models are usually expressed in terms of an equilibrium gating function,

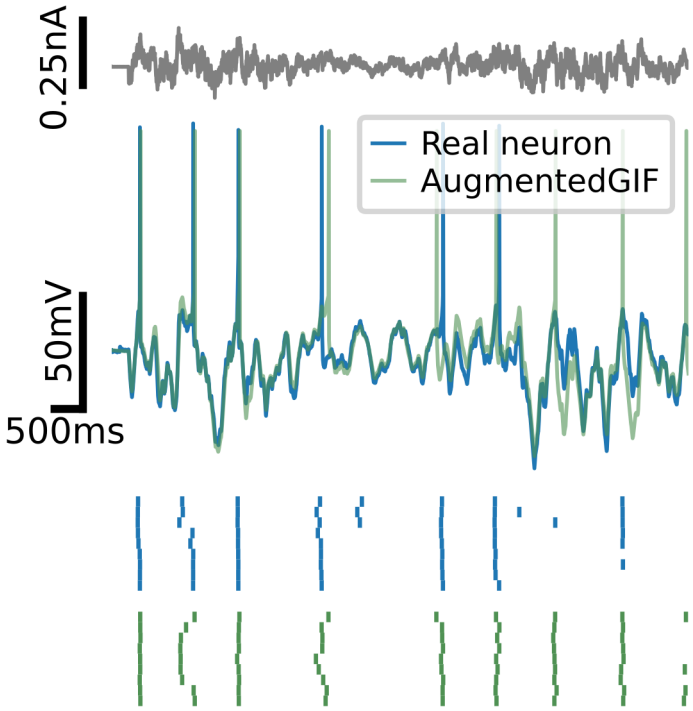

Figure 4: A GIF model augmented with a voltage-dependent current fitted to a serotonin neuron. The noisy input stimulus at the top was not used during fitting. Notice that the augmented GIF model (teal) accurately predicts the subthreshold voltage (middle) and spike times (raster, bottom) of the real neuron (blue). The spike rasters at bottom are for several repetitions of the test stimulus shown at top. These illustrate that the augmented GIF model captures some of the natural stochasticity of spiking observed in serotonin neurons.

$a(t) = m(t)h(t)(V(t) - E_V)$. Substituting this back into Eq. 13, we obtain a definition of the voltage-dependent current in terms of a *known variable* scaled by an *unknown parameter*

$$I_V(t) = g_V a(t). \tag{14}$$

Recall from Section 3.3 that the unknown parameters in the subthreshold component of the GIF model can be found easily as long as the subthreshold dynamics can be written in a linear form; in other words, as a sum of known variables scaled by unknown parameters. Substituting Eq. 14 back into Eq. 12 and expanding and rearranging the terms, we obtain the following linear form in analogy with Eq. 11

$$\widehat{\frac{dV}{dt}} = \frac{\widehat{g}_l \widehat{E}_l}{\widehat{C}} + \frac{-\widehat{g}_l}{\widehat{C}} V(t) + \frac{\widehat{g}_V}{\widehat{C}} a(t) + \frac{1}{\widehat{C}} I_{\text{ext}}(t) + \frac{-\widehat{w}_1^{(\eta)}}{\widehat{C}} \sum_{\{s \in \mathcal{S}; s<t\}} e^{\frac{s-t}{\tau_1^{(\eta)}}} + \cdots + \frac{-\widehat{w}_k^{(\eta)}}{\widehat{C}} \sum_{\{s \in \mathcal{S}; s<t\}} e^{\frac{s-t}{\tau_k^{(\eta)}}}.$$

Because the subthreshold dynamics can still be written in a linear form, the regression approach to estimating the unknown model parameters presented in Section 3.3 can still be used, ultimately yielding an augmented GIF model with a voltage-dependent ionic current (see Fig. 3)[4].

Augmenting the GIF model with additional components such as ionic currents can bring the assumptions of the neuron model into closer agreement with the known features of particular neurons. This improves

which is a sigmoidal function of voltage, and one or more gating time constants, which may themselves depend on voltage. Readers with a background in whole-cell electrophysiology will likely already be familiar with techniques for measuring these quantities. For a comprehensive treatment, see Hille (2001).

[4]For an example of a similar approach used to estimate the parameters of ionic currents in a more detailed model, see Huys, Ahrens, and Paninski (2006).

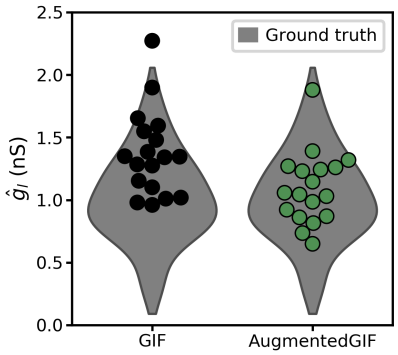

Figure 5: Leak conductance estimated by GIF models fitted to serotonin neurons (circles). Ground-truth estimates for this parameter based on experimental measurements from a large number of cells are shown in gray; wider areas indicate a relatively greater proportion of cells. Notice that the estimates produced by the augmented GIF model are closer to the ground truth.

the interpretability of the model by reducing the extent to which multiple electrical features are mixed into a single model term. Evidence of this mixing can be seen in the estimated values of $\widehat{g}_l$ in serotonin neurons using the GIF model and its augmented counterpart presented above. Even though the leak term used to estimate $\widehat{g}_l$ is the same in both models, the values of $\widehat{g}_l$ in the augmented model are closer to the corresponding true values g_l because the effects of the voltage-dependent current are mixed into it to a lesser extent (see Fig. 5). Of course, unless the Hodgkin-Huxley model of the current used in the augmented GIF model is exactly correct, a certain amount of mixing will always occur, which explains why the distribution of $\widehat{g}_l$ in Fig. 5 does not exactly agree with the ground truth. This reduced mixing can also increase the accuracy of model predictions by decreasing the dependence of model parameter estimates on the input used to fit the model (as discussed in Section 3.1). In the case of serotonin neurons, the augmented GIF predicts the timing of spikes significantly more accurately than the base GIF model (Harkin et al. 2020), even though the differences between the two models are limited to the subthreshold dynamics. (See Fig. 4 for an example of an augmented GIF model fitted to a serotonin neuron.) These results illustrate how adjustments to the GIF model can improve accuracy and interpretability.

4 Summary

In this chapter, we have seen that generalized integrate-and-fire (GIF) models build on leaky integrate-and-fire models to capture three of the most fundamental features of neurons: leaky subthreshold integration, stochastic spiking, and spike-frequency adaptation. The simplified mathematical structure of the GIF model provides a one-to-one correspondence between model components and electrophysiological features, making it intuitive to understand. We also saw that the subthreshold and spiking components of the GIF model are rooted in linear models that are easily fitted to data. This allows the GIF model to be constrained to mimic the behaviour of individual neurons based on very little data using a two-step optimization procedure, often with better results than more labour-intensive experimental approaches that require measuring the values of model parameters one at a time. Finally, we showed how the linear components of the GIF model can be extended to account for non-linear ionic currents that are not present in the GIF model as it was initially defined.

5 Further reading

The leaky integrate-and-fire model as it is used today was first introduced by Stein (1965), and the generalized integrate-and-fire model as it is presented here was introduced by Mensi, Naud, et al. (2012). See Kobayashi (2009) for an earlier model similar to the GIF model which also captures a wide range of neural behaviours.

A detailed derivation of the GIF model and its two-step fitting procedure can be found in Gerstner et al. (2014). For a very practical description of how to carry out experiments that can be used to constrain the GIF model, and an overview of how GIF models can be fitted using publicly-available software, see Pozzorini et al. (2015). For examples of how different variations of the GIF framework can be used to capture the behaviours of various types of cortical neurons, see Mensi, Hagens, et al. (2016) and Teeter et al. (2018). The definitive textbook on the physiology of ion channels and neuronal membranes is Hille (2001).

The GIF modelling framework is conceptually related to other classes of neuron models that are based on linearity assumptions. Like the GIF framework, generalized linear models (GLMs) (Jonathan W. Pillow et al. 2008) and linear-nonlinear Poisson models (LNPs) (Truccolo et al. 2005) are based on a linear function of a set of inputs which is then passed through a non-linear link function to produce a firing rate (GLMs) or spike probability (LNPs). However, unlike GIF models, these models do not attempt to predict the subthreshold voltage as an intermediate step. This means that GLMs and LNPs are not well-suited to cases where the subthreshold voltage is of primary interest, or when spiking data is very sparse. On the other hand, these models can be fitted to spiking data even when the subthreshold voltage is not known, as is the case during extracellular recording.

In this chapter, we have introduced optimization methods that rely on either exact knowledge of the relationship between model parameter values and predictive accuracy to solve for the best possible parameter values directly, or that use only local knowledge of this relationship to find the best values within a neighbourhood (gradient-based methods introduced in Section 3.3). Gonçalves et al. (2020) recently introduced an intermediate approach which uses an artificial neural network to approximate the global relationship between parameter values and model outputs, allowing approximately optimal parameter values to be found even for complex models.

References

Balachandar, Arjun and Steven A. Prescott (2018). "Origin of heterogeneous spiking patterns from continuously distributed ion channel densities: a computational study in spinal dorsal horn neurons: Heterogeneous spiking patterns in spinal dorsal horn neurons". en. In: *The Journal of Physiology* 596.9, pp. 1681–1697.

"Estimating parameters of probabilistic neuron models" (2014). In: *Neuronal Dynamics*. 1st ed. Cambridge: Cambridge University Press, pp. 243–266.

Gerstner, Wulfram et al. (2014). *Neuronal Dynamics*. 1st ed. Cambridge: Cambridge University Press.

Golowasch, Jorge et al. (2002). "Failure of Averaging in the Construction of a Conductance-Based Neuron Model". en. In: *Journal of Neurophysiology* 87.2, pp. 1129–1131.

Gonçalves, Pedro et al. (2020). "Training deep neural density estimators to identify mechanistic models of neural dynamics". In: *eLife* 9, e56261.

Harkin, Emerson et al. (2020). "Preferential sensitivity to sudden inputs by serotonin neurons of the dorsal raphe nucleus". In: *Biorxiv*.

Hastie, Trevor, Robert Tibshirani, and Jerome Friedman (2009). "Model Assessment and Selection". In: *The Elements of Statistical Learning*. 2nd ed. Springer Series in Statistics. New York: Springer, pp. 219–260.

Hille, Bertil (2001). *Ion Channels of Excitable Membranes*. 3rd ed. Sunderland: Sinauer Associates.

Hodgkin, A. L. and A. F. Huxley (1952). "A Quantitative Description of Membrane Current and its Application to Conduction and Excutation in Nerve". In: *Journal of Physiology* 117, pp. 500–544.

Huys, Quentin J. M., Misha B. Ahrens, and Liam Paninski (2006). "Efficient Estimation of Detailed Single-Neuron Models". en. In: *Journal of Neurophysiology* 96.2, pp. 872–890.

Kobayashi, Ryota (2009). "Made-to-order spiking neuron model equipped with a multi-timescale adaptive threshold". en. In: *Frontiers in Computational Neuroscience* 3.

Kohavi, Ron (1995). "A Study of Cross-Validatoin and Bootstrap for Accuracy Estimation and Model Selection". en. In: *International Joint Conference on Artificial Intelligence*.

Lapicque, Louis (1907). "Recherches quantitatives sur l'excitation électrique des nerfs traitée comme une polarisation". In: *Journal de Physiologie et de Pathologie Générale* 9, pp. 620–635.

Lundstrom, Brian N et al. (2008). "Fractional differentiation by neocortical pyramidal neurons". en. In: *Nature Neuroscience* 11.11, pp. 1335–1342.

Mainen, Z. and T. Sejnowski (1995). "Reliability of spike timing in neocortical neurons". en. In: *Science* 268.5216, pp. 1503–1506.

Mensi, Skander, Olivier Hagens, et al. (2016). "Enhanced Sensitivity to Rapid Input Fluctuations by Nonlinear Threshold Dynamics in Neocortical Pyramidal Neurons". en. In: *PLOS Computational Biology* 12.2. Ed. by Ian H. Stevenson, e1004761.

Mensi, Skander, Richard Naud, et al. (2012). "Parameter extraction and classification of three cortical neuron types reveals two distinct adaptation mechanisms". en. In: *Journal of Neurophysiology* 107.6, pp. 1756–1775.

Paninski, Liam, Eero P Simoncelli, and Jonathan W Pillow (2004). "Maximum Likelihood Estimation of a Stochastic Integrate-and-Fire Neural Model". en. In: *Advances in Neural Information Processing Systems*, pp. 1311–1318.

Pillow, Jonathan W. et al. (2008). "Spatio-temporal correlations and visual signalling in a complete neuronal population". en. In: *Nature* 454.7207, pp. 995–999.

Pozzorini, Christian et al. (2015). "Automated High-Throughput Characterization of Single Neurons by Means of Simplified Spiking Models". en. In: *PLOS Computational Biology* 11.6. Ed. by Jonathan W. Pillow, e1004275.

Stein, Richard B. (1965). "A Theoretical Analysis of Neuronal Variability". en. In: *Biophysical Journal* 5.2, pp. 173–194.

Teeter, Corinne et al. (2018). "Generalized leaky integrate-and-fire models classify multiple neuron types". en. In: *Nature Communications* 9.1, p. 709.

Truccolo, Wilson et al. (2005). "A Point Process Framework for Relating Neural Spiking Activity to Spiking History, Neural Ensemble, and Extrinsic Covariate Effects". en. In: *Journal of Neurophysiology* 93.2, pp. 1074–1089.

Wolpert, D.H. and W.G. Macready (1997). “No free lunch theorems for optimization”. en. In: *IEEE Transactions on Evolutionary Computation* 1.1, pp. 67–82.